

Consistent forcing scheme in the cascaded lattice Boltzmann method

Linlin Fei¹, K. H. Luo^{1,2}

¹ Center for Combustion Energy; Key laboratory for Thermal Science and Power Engineering of Ministry of Education, Department of Thermal Engineering, Tsinghua University, Beijing 100084, China

² Department of Mechanical Engineering, University College London, Torrington Place, London WC1E 7JE, UK

(Dated: June 5, 2017)

In this paper, we give a more pellucid derivation for the cascaded lattice Boltzmann method (CLBM) based on a general multiple-relaxation-time (MRT) frame through defining a shift matrix. When the shift matrix is a unit matrix, the CLBM degrades into an MRT LBM. Based on this, a consistent forcing scheme is developed for the CLBM. The applicability of the non-slip rule, the second-order convergence rate in space and the property of isotropy for the consistent forcing scheme is demonstrated through the simulation of several canonical problems. Several other existing force schemes previously used in the CLBM are also examined. The study clarifies the relation between MRT LBM and CLBM under a general framework.

PACS numbers: 47.11.-j, 05.20.Dd

I. INTRODUCTION

The lattice Boltzmann method (LBM), based on the simplified kinetic models, has gained remarkable success for the simulation of complex fluid flows and beyond, with applications (but not limited to) to micro flows, flows in porous media, turbulence, and multiphase flows [1–6]. The LBM solves a specific discrete Boltzmann equation for the distribution functions, designed to recover the Navier-Stokes (N-S) equations in the macroscopic limit. The meso-scale nature of LBM allows its natural incorporation of micro and meso-scale physics, while the highly efficient algorithm makes it affordable computationally [7].

In the standard “collision-streaming” LBM algorithm, the simplest collision operator is the Bhatnagar-Gross-Krook (BGK) or single-relaxation-time (SRT) operator, which relaxes all the distribution functions to their local equilibrium counterparts at a common rate and the relaxation rate is related to the kinematic viscosity [8]. The multiple-relaxation-time (MRT) operator is another extensively used operator [9], in which the collision is executed in the moment space and the relaxation rates for different moments can be different. More recently, a central-moments-based or cascaded operator was proposed by Geier *et al.* [10]. In the cascaded lattice Boltzmann method (CLBM), the collision is carried out in the space of central moment rather than that of raw moment as in the MRT LBM. Compared with the BGK operator, the MRT and cascaded operators can increase the numerical stability significantly [10–13]. Although the collision steps in these LBMs are quite different, the streaming steps are carried out in the same way by streaming the post-collision distributions to their neighbors. It should be noted that other collision operators, like the two-relaxation-time (TRT) operator [14, 15] and the entropic operator [16, 17] are also very popular in the lattice

Boltzmann community.

In many fluid systems, an external or internal force field plays an important role in the flow behaviours. To incorporate the force effect, different force treatments have been proposed in the literature [4, 18–20]. In 2002, Guo *et al* analyzed the discrete lattice effects on the forcing scheme and developed a representation of the forcing term [21]. Guo *et al.* then extended the method to the MRT LBM in 2008 [22]. Up to now, the method by Guo *et al* has been widely used in the LBM simulation. For the CLBM simulation, there is still no commonly used forcing scheme, while one scheme by method of central moments has been proposed by Premnath *et al.* [23]. In Ref. [24], Lycett-Brown and Luo incorporate the forcing scheme for the BGK LBM into the CLBM directly. As analysed by De Rosis [25], the method proposed by Premnath *et al* may encounter cumbersome practical implementations. Based on the central moments of a discrete equilibrium, a forcing scheme has been developed in [25].

However, there is still no analysis about whether these forcing schemes in the CLBM are consistent with the forcing scheme in the MRT LBM [22] and the original scheme proposed by Guo *et al* in the BGK LBM [21]. In this paper, we propose a more pellucid derivation for the CLBM by defining a shift matrix. This definition clarifies the relationship between MRT LBM and CLBM. Based on this frame, we present a consistent forcing scheme in CLBM, and show that the previous methods in Refs. [23–25] are not consistent. The rest of the paper is structured as follows: Section II gives the new derivation for the cascaded LBM and presents the consistent forcing scheme. Section III presents a short analysis for the previous forcing schemes. Numerical verifications are presented in Sec. IV. Finally, conclusions of this work are made in Sec. V.

II. CASCADED LBM AND CONSISTENT FORCING SCHEME

A. Cascaded LBM

Without losing the generality, the D2Q9 lattice [8] is adopted here. The lattice speed $c = \Delta x/\Delta t = 1$ and the lattice sound speed $c_s = 1/\sqrt{3}$ are adopted, in which Δx and Δt are the lattice spacing and time step. The discrete velocities $\mathbf{e}_i = [|e_{ix}\rangle, \langle e_{iy}|]$ are defined as

$$\begin{aligned} |e_{ix}\rangle &= [0, 1, 0, -1, 0, 1, -1, -1, 1]^\top, \\ |e_{iy}\rangle &= [0, 0, 1, 0, -1, 1, 1, -1, -1]^\top. \end{aligned} \quad (1)$$

where $i = 0..8$, $|\cdot\rangle$ denotes a nine-dimensional column vector, and the superscript \top denotes the transposition.

Here we propose a new derivation for the CLBM, which is different from and more intelligible than that given by Geier *et al* [10]. We first define the raw and central velocity moments of the discrete distribution function (DF) f_i ,

$$\begin{aligned} k_{mn} &= \langle f_i | e_{ix}^m e_{iy}^n \rangle, \\ \tilde{k}_{mn} &= \langle f_i | (e_{ix} - u_x)^m (e_{iy} - u_y)^n \rangle, \end{aligned} \quad (2)$$

where u_x and u_y are the horizontal and vertical velocity components. The equilibrium values k_{mn}^{eq} and \tilde{k}_{mn}^{eq} are defined analogously by using the discrete equilibrium

distribution function (EDF) f_i^{eq} in Eq. (2). In the previous CLBM, the recombined raw moments are adopted,

$$|T_i\rangle = [k_{00}, k_{10}, k_{01}, k_{20} + k_{02}, k_{20} - k_{02}, k_{11}, k_{21}, k_{12}, k_{22}]^\top, \quad (3)$$

so do the recombined central moments \tilde{T}_i . The transformation from the discrete DF to its raw moments can be realized through a transformation matrix \mathbf{M} , and the shift from the raw moments to central moments can be realized through a shift matrix \mathbf{N} ,

$$\begin{aligned} |T_i\rangle &= \mathbf{M} |f_i\rangle, \\ |\tilde{T}_i\rangle &= \mathbf{N} |T_i\rangle. \end{aligned} \quad (4)$$

The explicit forms for \mathbf{M} and \mathbf{N} can be obtained through the definition in Eqs. (2,3,4). Explicitly, the transformation matrix \mathbf{M} is expressed as [24]

$$\mathbf{M} = \begin{bmatrix} 1 & 1 & 1 & 1 & 1 & 1 & 1 & 1 & 1 \\ 0 & 1 & 0 & -1 & 0 & 1 & -1 & -1 & 1 \\ 0 & 0 & 1 & 0 & -1 & 1 & 1 & -1 & -1 \\ 0 & 1 & 1 & 1 & 1 & 2 & 2 & 2 & 2 \\ 0 & 1 & -1 & 1 & -1 & 0 & 0 & 0 & 0 \\ 0 & 0 & 0 & 0 & 0 & 1 & -1 & 1 & -1 \\ 0 & 0 & 0 & 0 & 0 & 1 & 1 & -1 & -1 \\ 0 & 0 & 0 & 0 & 0 & 1 & -1 & -1 & 1 \\ 0 & 0 & 0 & 0 & 0 & 1 & 1 & 1 & 1 \end{bmatrix}, \quad (5)$$

and the shift matrix \mathbf{N} is given by

$$\mathbf{N} = \begin{bmatrix} 1 & 0 & 0 & 0 & 0 & 0 & 0 & 0 & 0 \\ -u_x & 1 & 0 & 0 & 0 & 0 & 0 & 0 & 0 \\ -u_y & 0 & 1 & 0 & 0 & 0 & 0 & 0 & 0 \\ u_x^2 + u_y^2 & -2u_x & -2u_y & 1 & 0 & 0 & 0 & 0 & 0 \\ u_x^2 - u_y^2 & -2u_x & 2u_y & 0 & 1 & 0 & 0 & 0 & 0 \\ u_x u_y & -u_y & -u_x & 0 & 0 & 1 & 0 & 0 & 0 \\ -u_x^2 u_y & 2u_x u_y & u_x^2 & -u_y/2 & -u_y/2 & -2u_x & 1 & 0 & 0 \\ -u_y^2 u_x & u_y^2 & 2u_x u_y & -u_x/2 & u_x/2 & -2u_y & 0 & 1 & 0 \\ u_x^2 u_y^2 & -2u_x u_y^2 & -2u_y u_x^2 & u_x^2/2 + u_y^2/2 & u_y^2/2 - u_x^2/2 & 4u_x u_y & -2u_y & -2u_x & 1 \end{bmatrix}. \quad (6)$$

In the collision step for the cascaded LBM, the central moments (\tilde{T}_i) of the discrete DF f_i are relaxed to their equilibrium values \tilde{T}_i^{eq} . Thus the post-collision central moments are

$$\begin{aligned} |\tilde{T}_i^*\rangle &= (\mathbf{I} - \mathbf{S}) |\tilde{T}_i\rangle + \mathbf{S} |\tilde{T}_i^{eq}\rangle \\ &= (\mathbf{I} - \mathbf{S}) \mathbf{N} \mathbf{M} |f_i\rangle + \mathbf{S} \mathbf{N} \mathbf{M} |f_i^{eq}\rangle. \end{aligned} \quad (7)$$

where $\mathbf{S} = \text{diag}(s_0, s_1, s_1, s_b, s_2, s_2, s_3, s_3, s_4)$ is a diagonal relaxation matrix. The kinematic and bulk viscosities are related to the relaxation parameters $s_2 = 1/(3\nu + 0.5)$ and $s_b = 1/(3\xi + 0.5)$, respectively. As recommended in Refs. [10, 23, 24], the equilibrium central moments of the discrete (EDF) f_i^{eq} are set equal to the continuous central moments of the Maxwellian-Boltzmann distribution

in continuous velocity space. To be specific,

$$|\tilde{T}_i^{eq}\rangle = [\rho, 0, 0, 2\rho c_s^2, 0, 0, 0, 0, \rho c_s^4]^\top, \quad (8)$$

where ρ is the fluid density, thus the matrix manipulation is not needed for $|\tilde{T}_i^{eq}\rangle$. The corresponding discrete EDF f_i^{eq} is in fact a generalized local equilibrium [23, 26]. Due to the definitions of the transformation and shift matrices, both of them are reversible (explicit expressions for \mathbf{M}^{-1} and \mathbf{N}^{-1} are given in the Appendix). The post-collision discrete DF is given by

$$|f_i^*\rangle = \mathbf{M}^{-1} \mathbf{N}^{-1} |\tilde{T}_i^*\rangle. \quad (9)$$

In the streaming step, the post-collision discrete DF in

space \mathbf{x} and time t streams to its neighbor in the next time step as usual [21, 22, 27],

$$f_i(\mathbf{x} + \mathbf{e}_i \Delta t, t + \Delta t) = f_i^*(\mathbf{x}, t). \quad (10)$$

Using the Chapman-Enskog analysis, the incompressible N-S equations can be reproduced in the low-Mach number limit [23, 24]. The hydrodynamics variables are obtained as,

$$\rho = \sum_i f_i, \quad \rho \mathbf{u} = \sum_i f_i \mathbf{e}_i. \quad (11)$$

It can be found that when the shift matrix \mathbf{N} is a unit matrix, the CLBM degrades into a non-orthogonal MRT LBM [27]. Thus the present derivation is based on a general multiple-relaxation-time frame and clarifies the relationship between the MRT LBM and CLBM.

B. Consistent forcing scheme

Inspired by the method proposed by Guo *et al* [21, 22], to incorporate an external or internal force field $\mathbf{F} = [F_x, F_y]$ into the CLBM, the collision step for central moments in Eq. (6) is modified by

$$\begin{aligned} |\tilde{T}_i^* \rangle &= (\mathbf{I} - \mathbf{S}) |\tilde{T}_i \rangle + \mathbf{S} |\tilde{T}_i^{eq} \rangle + (\mathbf{I} - \mathbf{S}/2) |C_i \rangle \\ &= \mathbf{N} \mathbf{M} |f_i \rangle + \mathbf{S} \mathbf{N} \mathbf{M} |f_i^{eq} \rangle + (\mathbf{I} - \mathbf{S}/2) \mathbf{N} \mathbf{M} |R_i \rangle \end{aligned} \quad (12)$$

where R_i is the force effect term, which can be obtained by [28],

$$R_i = \frac{\mathbf{F}}{\rho} \cdot \frac{(\mathbf{e}_i - \mathbf{u})}{c_s^2} f_i^{eq}. \quad (13)$$

When using the generalized local equilibrium, the central moments for $|R_i \rangle$ can be computed as,

$$|C_i \rangle = [0, F_x, F_y, 0, 0, 0, c_s^2 F_x, c_s^2 F_y, 0]^\top, \quad (14)$$

so the explicit formulation and matrix manipulation for $|R_i \rangle$ in Eq. (12) are not needed in the practical implementation. Then the fluid velocity is defined by,

$$\rho \mathbf{u} = \sum_i f_i \mathbf{e}_i + \frac{\Delta t}{2} \mathbf{F}. \quad (15)$$

Remark 1. In Eq. (12), the forcing effects in the present scheme are considered by means of central moments, which is compatible with the basic ideology (collision in the central moments space) in the CLBM.

Remark 2. When the shift matrix \mathbf{N} in Eq. (12) is a unit matrix, the CLBM with the present forcing scheme will degrade into the MRT LBM proposed by Liu *et al.* [27] with some high-order terms. It is known that the method of Liu *et al.* is equivalent to the method of Guo *et al.* in [22].

Remark 3. In the original forcing scheme proposed by Guo *et al.* [21], the forcing effect term is defined by R_{Gi} =

$w_i [(\mathbf{e}_i - \mathbf{u})/c_s^2 + (\mathbf{e}_i \cdot \mathbf{u}) \mathbf{e}_i/c_s^4] \mathbf{F}$. It is easy to find that the forcing effect term in Eq. (13) is equivalent to R_{Gi} plus some high-order terms. The constraint conditions for the forcing effect term (see Eq. (7) in [21]) are also satisfied in the present scheme. In particular, when all the parameters in the matrix \mathbf{S} are set equal to s_2 , the CLBM with the present forcing scheme will degrade into the BGK LBM with forcing scheme by Guo *et al.* in [21] with a generalized local equilibrium.

Remark 4. It is also found (see in Sec. IV) that the zero-slip velocity boundary condition for the half-way bounce-back rule ($s_3 = (16 - 8s_2)/(8 - s_2)$) discussed in [22, 29] is also applicable to the present forcing scheme.

From the above, we name the present forcing scheme as a consistent scheme in the CLBM.

III. OTHER FORCING METHODS

In this section, several other methods to incorporate forcing effects into the CLBM in the literature are summarized. To show the inconsistencies in these methods, they are all written in the general multiple-relaxation-time frame proposed in Sec. II A.

A. Forcing scheme by Premnath *et al.*

In 2009, Premnath *et al.* [23] proposed a forcing scheme to incorporate forcing terms into CLBM. Inspired by He *et al.* [28], they proposed a change of continuous distribution function f due to the presence of a force field,

$$\Delta f = \frac{\mathbf{F}}{\rho} \cdot \frac{(\mathbf{e}_i - \mathbf{u})}{c_s^2} f^M, \quad (16)$$

where f^M is the Maxwellian-Boltzmann distribution in continuous velocity space. The central moments of Δf is then incorporated into the collision stage in central moments by,

$$|\tilde{T}_i^* \rangle = (\mathbf{I} - \mathbf{S}) |\tilde{T}_i \rangle + \mathbf{S} |\tilde{T}_i^{eq} - C_{Pi}/2 \rangle. \quad (17)$$

The discrete counterpart of Δf is also needed to obtain the post-collision discrete DF,

$$|f_i^* \rangle = \mathbf{M}^{-1} \mathbf{N}^{-1} |\tilde{T}_i^* \rangle + |\Delta f_i \rangle \quad (18)$$

The fluid velocity is defined as in Eq. (15).

It should be noted that the original derivation in [23] is tedious, and C_{Pi} and Δf_i are corresponding to $\hat{\sigma}_{x^m y^n}$ and S_a in [23], respectively. Though the method is compatible with the central-moment-based collision operator, the explicit formulations of Δf_i and its raw moments are needed, which makes the practical implementations cumbersome [25]. Moreover, in their definition for the central

moments of Δf , they removed the high-order nonzero terms arbitrarily,

$$|C_{Pi}\rangle = [0, F_x, F_y, 0, 0, 0, 0, 0]^\top. \quad (19)$$

Though they think that the high-order terms do not affect consistency, we certainly see some inconsistencies. For example, the first element in Δf_i and R_{Gi} are apparently inconsistent,

$$\begin{aligned} \Delta f_0 &= -2F_x u_x - 2F_y u_y + O(u^3), \\ R_{G0} &= -3F_x u_x - 3F_y u_y, \end{aligned} \quad (20)$$

which will affect numerical performances (see in Sec. IV).

B. Forcing scheme by Lycett-Brown and Luo

Cascaded LBM was first used to simulated multiphase flows by Lycett-Brown *et al.* [24] in 2014. In their method, three forcing schemes, the Shan-Chen method [4], the EDM method [30] and Guo method [21] were adopted directly in the CLBM.

As discussed in the literature [31, 32], both the Shan-Chen method and EDM method obtain some additional terms in the recovered macroscopic equations. These additional terms may have some positive effects on the numerical performance of the Shan-Chen model [4], but it is not sensible to use the Shan-Chen method and EDM method in the CLBM directly for general flows. In the present work, we only consider the CLBM with the forcing scheme of Guo *et al.* Thus the collision stage in central moments can be written as,

$$|\tilde{T}_i^*\rangle = (\mathbf{I} - \mathbf{S}) |\tilde{T}_i\rangle + \mathbf{S} |\tilde{T}_i^{eq}\rangle + (1 - s_2/2)\mathbf{NM} |R_{Gi}\rangle, \quad (21)$$

while the fluid velocity is also defined as in Eq. (15).

C. Forcing scheme by De Rosiis

Recently, De Rosiis proposed an alternative method to incorporate forcing effects into the CLBM. The collision stage in central moments is,

$$|\tilde{T}_i^*\rangle = (\mathbf{I} - \mathbf{S}) |\tilde{T}_i\rangle + \mathbf{S} |\tilde{T}_i^{eq}\rangle + \frac{1}{2} |\xi_i\rangle, \quad (22)$$

where, ξ_i is the central moment of the forcing effect term, and the fluid velocity is also defined as in Eq. (15).

Unfortunately, there is a typographical error in Eq. (16) of the paper [25]. Particularly, the sign in front of $\xi_i/2$ is not correct. In this method, the forcing term is defined by the truncated local equilibrium DF, which gives a lot of velocity terms in ξ_i (see Eq. (15) in [25]). Due to the definition of central moments, it is not recommended to include velocity terms in ξ_i . Thus there are some spurious effects in this method. It is also noted that the computational load for ξ_i is much higher than

that of C_i in Eq. (14). Comparing Eq. (22) with Eq. (12), it is seen that the relaxation rate for each element of ξ_i is 1.0 in this method, which is not consistent with the multiple-relaxation-time ideology in the CLBM.

Remark 5. In the CLBM, the first three central moments are conserved moments, corresponding to conservations of mass and momentum. Thus the first two parameters (s_0 and s_1) in the relaxation matrix \mathbf{S} can be chosen freely. This property is retained in the present forcing scheme and the method by Premnath *et al.*, because the relaxation matrix acts on the forcing effect terms in these two methods (see Eq. (12) and Eq. (17)). However, s_1 need to be set equal to s_2 in method by Lycett-Brown and Luo, and to be 1.0 method by De Rosiis, to guarantee the conservation of momentum.

Remark 6. If s_3 is chosen to be 2.0, the forcing effect on the third-order central moment in Eq. (11) is removed. Thus the present scheme degrades into the forcing scheme by Premnath *et al.* only when $s_3 = 2.0$. Similarly, only when $s_3 = 1.0$, the difference between the forcing scheme by De Rosiis and the present scheme can be removed. And in the BGK limitation, all the parameters are equal to s_2 , at which the present scheme degrades into the method by Lycett-Brown and Luo.

Remark 7. In 2015, an improved forcing scheme for the pseudopotential model in multiphase flow was proposed by Lycett Brown and Luo [33]. The improved forcing scheme was then incorporated into the CLBM for multiphase flow with large-density-ratio at high Reynolds and Weber numbers [12]. The basic philosophy of the improved forcing scheme is making artificial errors in the pressure tensor to counteract the lack of thermodynamical consistency in the original pseudopotential model. Thus it is not suitable for general flows with a force field. Besides, another simple forcing term was used in CLBM to simulate turbulent channel flow in 2011 [34]. However, as analysed by Guo *et al.* [21], the method used in [34] can not recover the accurate macroscopic equations with a spatial and temporal variational force field in the BGK LBM, not to mention in the CLBM.

IV. NUMERICAL SIMULATIONS

In these section, we conduct several benchmark cases to verify the consistent forcing scheme. The other three methods mentioned in Sec. III are also used to validate our arguments. The three methods and present method are denoted by M_1 , M_2 , M_3 and M_p , respectively. In the simulation, s_1 is set to be s_2 in M_2 , but to be 1.0 in other methods.

A. Steady Poiseuille flow

The first problem considered is a steady Poiseuille flow driven by a constant body force \mathbf{F} . The flow direction is

set to be positive direction of the x axial, thus $\mathbf{F} = [F_x, 0]$. The analytical solution for a channel of width $2L$ is,

$$\mathbf{u}_a = \left[\frac{F_x}{2\nu} \left(1 - \frac{y^2}{L^2}\right), 0 \right]. \quad (23)$$

The periodic boundary conditions are used in the flow direction, while the standard half-way bounce-back boundary scheme is used for non-slip boundary conditions at the walls. Due to the simple flow property, the length of the channel is set to $3\Delta x$ to save the computational load.

As analysed by previous researchers [22, 29], when the relaxation rate for the energy flux is chosen to be $s_3 = (16 - 8s_2)/(8 - s_2)$, no numerical slips occurs in the Poiseuille flows for the MRT LBM. To check its applicability in the CLBM with the present forcing scheme, we first choose kinematic viscosity $\nu = 0.5$, $F_x = 0.01$, and only three nodes are used to cover the channel width ($2L = 3\Delta x$). We change s_3 from 0.2 to 1.8 with a 0.05 interval, and the other parameters are set equal to s_2 . The residual error $E_R < 1 \times 10^{-9}$ is used as the convergent criterion, and the relative error E_2 is calculated for the following analysis,

$$E_R = \sqrt{\frac{\sum (\mathbf{u}_{(t+1000\delta t)} - \mathbf{u}_t)^2}{\sum \mathbf{u}_{(t+1000\delta t)}^2}}, \quad E_2 = \sqrt{\frac{\sum (\mathbf{u} - \mathbf{u}_a)^2}{\sum \mathbf{u}_a^2}}. \quad (24)$$

For this case, the needed value for non-slip rule of s_3 is 1.6. As shown in Fig. 1, the relative error for each method changes with different values of s_3 . But only in the present method, the minimum value of E_2 is achieved when $s_3 = 1.6$. And when the non-slip condition is satisfied, the relative error reaches a quite small value even in a very coarse mesh.

To further confirm the consistent non-slip boundary condition in the present method, we conduct several others cases. Now the channel width is set to be 50 nodes, and different body forces $F_x = [1 \times 10^{-6}, 3 \times 10^{-6}, 5 \times 10^{-6}, 7 \times 10^{-6}]$ are considered. The configurations are the same as those in [23], s_3 is chosen according to the non-slip rule, while other relaxation parameters are 1.754. As shown in Table I, the relative errors for M_1 are $O(10^{-4})$, which is consistent with the results in [23], where the non-slip rule was not considered. Compared with these three methods, the relative errors for the present method are much smaller with 5-6 orders, which confirms the availability of the non-slip rule in the present method. For the differences between the three methods in this case, it is easy to analyze that the error terms in the three methods are in a descending order of M_1 , M_2 , and M_3 .

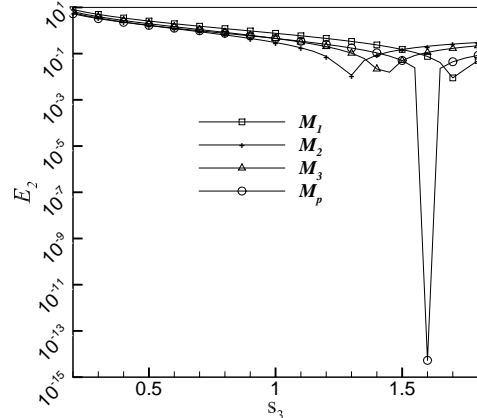


FIG. 1. E_2 changes with s_3 for different methods.

TABLE I. $E_2(\times 10^4)$ with different magnitudes of force for different methods.

F_x	M_1	M_2	M_3	M_p
1×10^{-6}	2.739	2.339	1.113	1.044×10^{-6}
3×10^{-6}	2.739	2.339	1.113	3.173×10^{-6}
5×10^{-6}	2.739	2.339	1.113	5.527×10^{-6}
7×10^{-6}	2.739	2.339	1.113	7.296×10^{-6}

B. Steady Taylor-Green flow

For the two-dimensional steady incompressible flow in a periodic box $N \times N$, if the force field is given by,

$$\mathbf{F}(x, y) = 2\nu u_0 \phi^2 [\cos(\phi x) \cos(\phi y), \sin(\phi x) \sin(\phi y)], \quad (25)$$

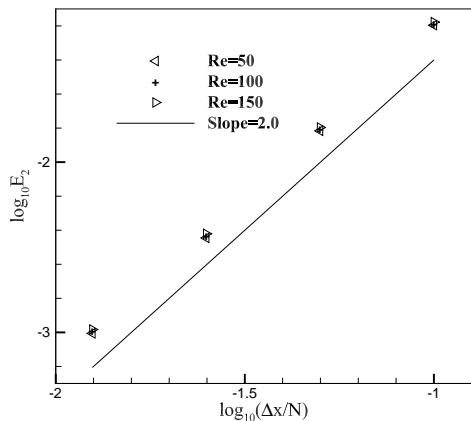
the flow has the following analytical solution,

$$\begin{aligned} \mathbf{u}_a(x, y) &= u_0 [\sin(\phi x) \sin(\phi y), \cos(\phi x) \cos(\phi y)], \\ p_a(x, y) &= p_0 + 0.25u_0^2 [\cos(2\phi x) - \cos(2\phi y)], \end{aligned} \quad (26)$$

where $\phi = 2\pi/N$, $p_0 = \rho_0 c_s^2$ and $\rho_0 = 1$. The flow is known as steady Taylor-Green flow or four-rolls mill [35], and is characterized by Reynolds number, $\text{Re} = u_0 \pi / \nu$. In the simulation, the computational domain covered by a series of grid nodes, $N/\Delta x = [10, 20, 40, 80]$, with three different conditions at $\text{Re} = [50, 100, 150]$. To weaken the artificial compressibility, $u_0 = 0.05$ is used in all the cases, s_b is given equal to s_2 , while the remaining relaxation parameters are set to unity. The relative error E_2 is computed from Eq. (24). The relationship between grid size and E_2 of the present forcing scheme at different Reynolds numbers is presented in Fig. 2. The slopes at $\text{Re} = 50, 100$ and 150 are 2.0133, 2.0076 and 2.0068, respectively. This demonstrates the scheme proposed has second-order accuracy in space. The relative error for each method is shown in Table II. It is found that the present scheme achieves the smallest relative error for every grid resolution at every Reynolds number. Due to

TABLE II. $E_2(\times 10^2)$ and convergence rates (CR) for different forcing methods with different values of Reynolds number.

$N/\Delta x$	Re = 50				Re = 100				Re = 150			
	M_P	M_1	M_2	M_3	M_P	M_1	M_2	M_3	M_P	M_1	M_2	M_3
10	6.3752	6.5748	6.5522	6.3959	6.5448	6.6456	6.6398	6.5660	6.6482	6.7162	6.7135	6.6698
20	1.5275	1.6263	1.6051	1.5538	1.5788	1.6283	1.6227	1.6063	1.5974	1.6305	1.6279	1.6261
40	0.3587	0.3969	0.3782	0.3843	0.3719	0.3961	0.3909	0.4074	0.3796	0.3957	0.3933	0.4145
80	0.0986	0.1141	0.1037	0.1498	0.1025	0.1109	0.1076	0.1543	0.1040	0.1098	0.1082	0.1560
CR	2.0133	1.9579	2.0031	1.8264	2.0076	1.9753	1.9896	1.8213	2.0068	1.9848	1.9917	1.8222

FIG. 2. E_2 changes with grid size for the present scheme at $Re = 50, 100$ and 150 .

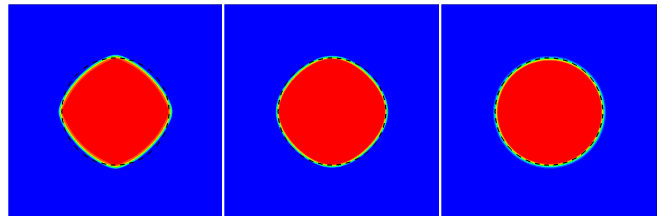
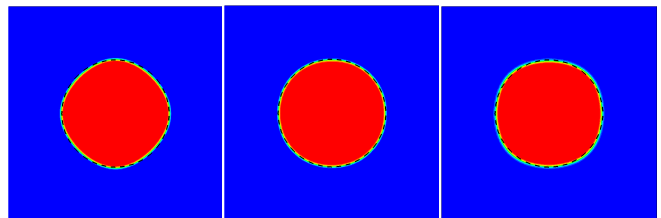
the discrete equilibrium central moments used in M_3 (see Eq. (10) in [36]), some additional errors are introduced into the CLBM, and this effect becomes evident when the mesh size is small. It is the reason why this method manifests an outlier for the finest grid resolution. Generally, each method presents a second-order convergence rate.

C. Single static droplet

To validate the availability of the present forcing scheme for a complex force field. We consider the simulations of a static droplet using the Shan-Chen multiphase model [4], which is also known as the pseudopotential approach in the multiphase flow. The interaction force is calculated from an interaction potential $\psi(x)$ [4],

$$\mathbf{F} = -G\psi(x) \sum_i w_i \psi(x + e_i \Delta t) e_i \quad (27)$$

where G is used to control the interaction strength and w_i are the weights. When only the nearest-neighbor interactions are considered on the D2Q9 lattice, $w_i = 1/3$ for $|e_i|^2 = 1$ and $w_i = 1/12$ for $|e_i|^2 = 2$. The exponential form of the pseudopotential is used, i.e., $\psi(\rho) =$

FIG. 3. Steady-state density contours given by M_1 with $s_3 = [1.0, 1.4, 1.8]$.FIG. 4. Steady-state density contours given by M_2 with $s_3 = [1.0, 1.4, 1.8]$.

$\psi_0 \exp(-\rho_0/\rho)$. Let us denote ρ_V and ρ_L as the vapor and liquid coexistence densities, respectively. In this study, $\psi_0 = 1$, $\rho_0 = 1$ and $G = 10/3$ are used, which leads to $\rho_V = 0.3675$ and $\rho_L = 2.783$ [37, 38]. The simulations are conducted in a periodic box $N \times N = 200 \times 200$. A circle droplet of radius R is initialized by setting $\rho = \rho_L$ in the circle and $\rho = \rho_V$ outside the circle. The relaxation parameters are chosen as $s_b = s_v = 1.4$, and $s_3 = [1.0, 1.4, 1.8]$.

Firstly, the steady-state density contours with $R = 50$ given by different forcing schemes are compared. The additional dashed circle represents the theoretical location of the droplet. It is found in Fig. 3 the shape of droplet is s_3 -dependent and it changes from a out-of-round shape to a circle with the increase of s_3 . As discussed in Sec. III A, the removal of high-order terms for the central moments of Δf in [23] makes inconsistencies with the scheme proposed by Guo *et al.* And only when s_3 is set to be 2.0, the inconsistency can be eliminated. Though we can not give the result with $s_3 = 2.0$ (divergent for

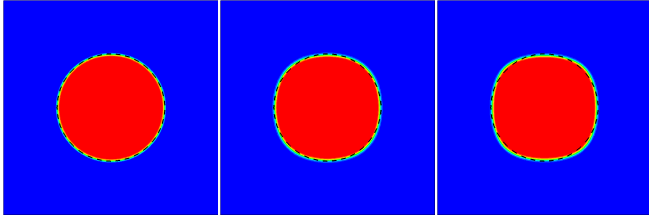


FIG. 5. Steady-state density contours given by M_3 with $s_3 = [1.0, 1.4, 1.8]$.

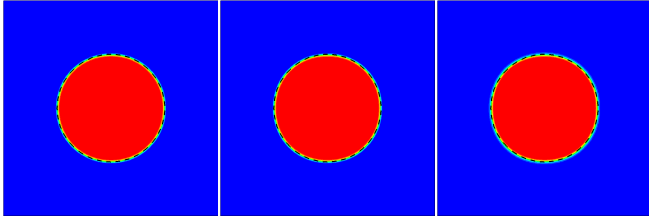


FIG. 6. Steady-state density contours given by present method with $s_3 = [1.0, 1.4, 1.8]$.

this simulation), the tendency confirms our argument. Analogously, as discussed in Sec. III B and Sec. III C, the inconsistencies in M_2 and M_3 can only be eliminated under the conditions of $s_3 = s_2$ and $s_3 = 1.0$, respectively. Thus the droplets in Fig. 4 and Fig. 5 become out-of-round when s_3 is not set the specific value. For the present forcing scheme, the droplets are always in round shapes rather than depend on the value of s_3 , as seen in Fig. 6. According to Laplace's law, the pressure difference between the pressure inside and the one outside a droplet is related to the surface tension γ and the droplet radius R via $\Delta p = \gamma/R$. To check the ability of repeating the Laplace's law, a series of static droplets with $R = [20, 25, 30, 35, 40, 45, 50]$ are simulated. The

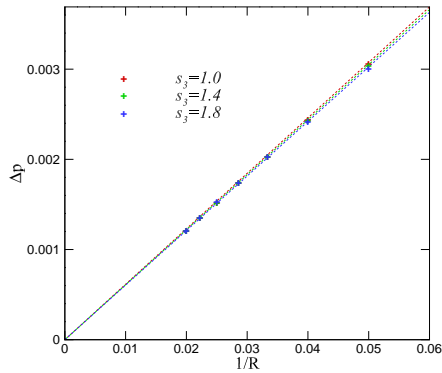


FIG. 7. Numerical validation of Laplace's law for the present forcing scheme.

pressure is computed through $p = \rho c_s^2 + G\psi^2/2$. As shown in Fig. 7, Laplace's law is well satisfied. The measured surface tensions for $s_3 = [1.0, 1.4, 1.8]$ are 0.0615, 0.0610 and 0.0605, respectively.

V. CONCLUSIONS

In this study, we present a more pellucid derivation of CLBM. A shift matrix \mathbf{N} is defined in the derivation, by which the raw moments of the discrete distribution function are shifted to their central moments. This definition clarifies the relationship between the MRT LBM and CLBM. Based on this, a new method of incorporating forcing terms into the CLBM is proposed.

The forcing effect term is incorporated by means of central moments, which is compatible with the basic ideology of the CLBM. According to the definition of the shift matrix \mathbf{N} , the CLBM degrades into the MRT LBM when \mathbf{N} is a unit matrix. The present forcing scheme retains the property of and degrades into the Guo forcing scheme in the MRT LBM when \mathbf{N} is a unit matrix. Specifically, the present forcing scheme degrades to the original forcing scheme proposed by Guo *et al* when all the relaxation parameters are set to the same. Numerical simulations for several benchmark problems confirm the applicability of the non-slip rule, the second-order accuracy in space and the property of isotropy for the present scheme. In the meantime, some inconsistencies in the previous models are also revealed.

The method developed is quite pellucid, and no cumbersome operations are involved in the practical implementation. Further work will demonstrate that the present scheme can be extended to three dimensions (3D) readily.

ACKNOWLEDGMENTS

Support from the MOST National Key Research and Development Programme (Project No. 2016YFB0600805) and the Center for Combustion Energy at Tsinghua University is gratefully acknowledged. Supercomputing time on ARCHER is provided by the UK Consortium on Mesoscale Engineering Sciences (UKCOMES) under the UK Engineering and Physical Sciences Research Council Grant No. EP/L00030X/1.

Appendix A: Appendixes

Analogously, the raw moments can be transformed to the discrete DF through \mathbf{M}^{-1} , and the central moments can be shifted to raw moments through \mathbf{N}^{-1} ,

$$\begin{aligned} |f_i\rangle &= \mathbf{M}^{-1} |T_i\rangle, \\ |T_i\rangle &= \mathbf{N}^{-1} |\tilde{T}_i\rangle. \end{aligned} \quad (\text{A1})$$

The explicit expressions for \mathbf{M}^{-1} and \mathbf{N}^{-1} are

$$\mathbf{M}^{-1} = \begin{bmatrix} 1 & 0 & 0 & -1 & 0 & 0 & 0 & 0 & 1 \\ 0 & 1/2 & 0 & 1/4 & 1/4 & 0 & 0 & -1/2 & -1/2 \\ 0 & 0 & 1/2 & 1/4 & -1/4 & 0 & -1/2 & 0 & -1/2 \\ 0 & -1/2 & 0 & 1/4 & 1/4 & 0 & 0 & 1/2 & -1/2 \\ 0 & 0 & -1/2 & 1/4 & -1/4 & 0 & 1/2 & 0 & -1/2 \\ 0 & 0 & 0 & 0 & 0 & 1/4 & 1/4 & 1/4 & 1/4 \\ 0 & 0 & 0 & 0 & 0 & -1/4 & 1/4 & -1/4 & 1/4 \\ 0 & 0 & 0 & 0 & 0 & 1/4 & -1/4 & -1/4 & 1/4 \\ 0 & 0 & 0 & 0 & 0 & -1/4 & -1/4 & 1/4 & 1/4 \end{bmatrix}, \quad (\text{A2})$$

and

$$\mathbf{N}^{-1} = \begin{bmatrix} 1 & 0 & 0 & 0 & 0 & 0 & 0 & 0 & 0 & 0 \\ u_x & 1 & 0 & 0 & 0 & 0 & 0 & 0 & 0 & 0 \\ u_y & 0 & 1 & 0 & 0 & 0 & 0 & 0 & 0 & 0 \\ u_x^2 + u_y^2 & 2u_x & 2u_y & 1 & 0 & 0 & 0 & 0 & 0 & 0 \\ u_x^2 - u_y^2 & 2u_x & -2u_y & 0 & 1 & 0 & 0 & 0 & 0 & 0 \\ u_x u_y & u_y & u_x & 0 & 0 & 1 & 0 & 0 & 0 & 0 \\ u_x^2 u_y & 2u_x u_y & u_x^2 & u_y/2 & u_y/2 & 2u_x & 1 & 0 & 0 & 0 \\ u_y^2 u_x & u_y^2 & 2u_x u_y & u_x/2 & -u_x/2 & 2u_y & 0 & 1 & 0 & 0 \\ u_x^2 u_y^2 & 2u_x u_y^2 & 2u_y u_x^2 & u_x^2/2 + u_y^2/2 & u_y^2/2 - u_x^2/2 & 4u_x u_y & 2u_y & 2u_x & 1 & 0 \end{bmatrix}. \quad (\text{A3})$$

- [1] Y.-H. Qian, S. Succi, and S. Orszag, *Annu. Rev. Comput. Phys* **3**, 195 (1995).
- [2] S. Chen and G. D. Doolen, *Annual review of fluid mechanics* **30**, 329 (1998).
- [3] S. Succi, *The lattice Boltzmann equation: for fluid dynamics and beyond* (Oxford university press, 2001).
- [4] X. Shan and H. Chen, *Physical Review E* **47**, 1815 (1993).
- [5] Z. Guo and C. Shu, *Lattice Boltzmann method and its applications in engineering*, Vol. 3 (World Scientific, 2013).
- [6] W. Gong, Y. Zu, S. Chen, and Y. Yan, *Science Bulletin* **62**, 136 (2016).
- [7] Q. Li, K. Luo, Q. Kang, Y. He, Q. Chen, and Q. Liu, *Progress in Energy and Combustion Science* **52**, 62 (2016).
- [8] Y. Qian, D. d’Humières, and P. Lallemand, *EPL (Europhysics Letters)* **17**, 479 (1992).
- [9] D. d’Humières, *Rarefied gas dynamics- Theory and simulations*, 450 (1994).
- [10] M. Geier, A. Greiner, and J. G. Korvink, *Physical Review E* **73**, 066705 (2006).
- [11] P. Lallemand and L.-S. Luo, *Physical Review E* **61**, 6546 (2000).
- [12] D. Lycett-Brown and K. H. Luo, *Physical Review E* **94**, 053313 (2016).
- [13] L. Fei and K. Luo, *arXiv preprint arXiv:1610.07114* (2016).
- [14] I. Ginzburg, *Advances in Water resources* **28**, 1171 (2005).
- [15] I. Ginzburg, F. Verhaeghe, and D. d’Humières, *Communications in computational physics* **3**, 427 (2008).
- [16] S. Ansumali, I. V. Karlin, and H. C. Öttinger, *EPL (Europhysics Letters)* **63**, 798 (2003).
- [17] S. Ansumali and I. V. Karlin, *Physical Review E* **62**, 7999 (2000).
- [18] X. He, S. Chen, and R. Zhang, *Journal of Computational Physics* **152**, 642 (1999).
- [19] J. M. Buick and C. A. Greated, *Physical Review E* **61**, 5307 (2000).
- [20] A. Ladd and R. Verberg, *Journal of Statistical Physics* **104**, 1191 (2001).
- [21] Z. Guo, C. Zheng, and B. Shi, *Physical Review E* **65**, 046308 (2002).
- [22] Z. Guo and C. Zheng, *International Journal of Computational Fluid Dynamics* **22**, 465 (2008).
- [23] K. N. Premnath and S. Banerjee, *Physical Review E* **80**, 036702 (2009).
- [24] D. Lycett-Brown and K. H. Luo, *Computers & Mathematics with Applications* **67**, 350 (2014).
- [25] A. De Rosis, *Physical Review E* **95**, 023311 (2017).
- [26] P. Asinari, *Phys Rev E* **78**, 016701 (2008).
- [27] Q. Liu, Y.-L. He, D. Li, and Q. Li, *International Journal of Heat and Mass Transfer* **102**, 1334 (2016).
- [28] X. He, S. Chen, and G. D. Doolen, *Journal of Computational Physics* **146**, 282 (1998).

- [29] I. Ginzburg and D. dHumières, *Physical Review E* **68**, 066614 (2003).
- [30] A. Kupershtokh, D. Medvedev, and D. Karpov, *Computers & Mathematics with Applications* **58**, 965 (2009).
- [31] H. Huang, M. Krafczyk, and X. Lu, *Physical Review E* **84**, 046710 (2011).
- [32] Q. Li, K. H. Luo, and X. J. Li, *Physical Review E* **86**, 016709 (2012).
- [33] D. Lycett-Brown and K. H. Luo, *Physical Review E* **91**, 023305 (2015).
- [34] R. K. Freitas, A. Henze, M. Meinke, and W. Schröder, *Computers & Fluids* **47**, 115 (2011).
- [35] G. Taylor, *Proceedings of the Royal Society of London. Series A, Containing Papers of a Mathematical and Physical Character* **146**, 501 (1934).
- [36] A. De Rosis, *EPL (Europhysics Letters)* **116**, 44003 (2017).
- [37] Z. Yu and L.-S. Fan, *Journal of Computational Physics* **228**, 6456 (2009).
- [38] Q. Li, P. Zhou, and H. Yan, *Physical Review E* **94**, 043313 (2016).